EO Africa // ARIES

D03 - State-of-the-art review report on the EO analysis method/s and algorithm/s

Version 1.0, February 2023

Contract No: 4000139191/22/I-DT

submitted by

	VISTA Remote Sensing in Geosciences GmbH (VISTA)
	Vlaamse Instelling voor Technologisch Onderzoek, Naamloze vennootschap (VITO)
	Luxemburg Institute of Science and Technology (LIST)

D03 - State-of-the-art review report on
the EO analysis method/s and
algorithm/s

ESA STUDY CONTRACT REPORT

ESA Contract No	SUBJECT		CONTRACTOR
4000139191/22/I-DT	EO Africa // ARIES		VISTA Remote Sensing in Geosciences GmbH (VISTA)

* ESA CR( )No	* STAR CODE	Vol.1	* ESA CR( )No

ABSTRACT:

This document reviews the State-of-the-art of EO analysis method/s and algorithm/s.

Version 1.0

Status: 07. February 2023

The work described in this report was done under ESA Contract. Responsibility for the contents resides in the author or organisation that prepared it.

Names of authors: Christoph Jörges (Vista), Jeroen Degerickx (Vito), Kanishka Mallick (LIST), Juan García Quijano (Vito) Veronika Otto (Vista), Silke Migdall (Vista)

** NAME OF ESA STUDY MANAGER	** ESA BUDGET HEADING
Mr. Z. Szantoi	
DIV: EOP-SDR	
DIRECTORATE: Earth Observation Programmes	

D03 - State-of-the-art review report on
the EO analysis method/s and
algorithm/s

Authors of report

The present report was prepared by:

Christoph Jörges, Veronika Otto

VISTA Geowissenschaftliche Fernerkundung GmbH

Gabelsbergerstr. 51, D-80333 Munich, Germany

Jeroen Degerickx, Juan García Quijano
Vlaamse Instelling voor Technologisch Onderzoek, Naamloze vennootschap
(VITO)

Kanishka Mallick
Luxembourg Institute of Science and Technology (LIST)

D03 - State-of-the-art review report on
the EO analysis method/s and
algorithm/s

Content

D03 - State-of-the-art review report on
the EO analysis method/s and
algorithm/s

Figures

D03 - State-of-the-art review report on
the EO analysis method/s and
algorithm/s

List of Acronyms

AHSI	Advanced Hyperspectral Imager
AL	Active learning
ANN	Artificial neural network
ASTER	Advanced Spaceborne Thermal Emission and Reflection Radiometer
AVHRR	Advanced Very High Resolution Radiometer
AVIRIS	Airborne Visible Infra Red Imaging Spectrometer
ASI	Agenzia Spaziale Italiana
CCC	Canopy Chlorophyll Content
CHIME	Copernicus Hyperspectral Imaging Mission for the Environment
CNC	Canopy Nitrogen Content
CRI	Carotenoid Reflectance Index
CTSD	Standard deviation of canopy temperature
CWC	Canopy Water Content
CWSI	Crop water stress index
DAR	Dirichlet Aggregation Regression
DESIS	DLR Earth Sensing Imaging Spectrometer
DLR	German Aerospace Center
DMS	Data mining sharpener
ECOSTRESS	Ecosystem Spaceborne Thermal Radiometer Experiment on Space Station
EnMAP	Environmental Mapping and Analysis Program
EO	Earth Observation
ESA	European Space Agency
ESI	Evaporative Stress Index
ET	Evapotranspiration
EWT	Equivalent Water Thickness
FAO	Food and Agricultural Organization of the United Nations
fAPAR	Fraction of absorbed photosynthetically active radiation
FMC	Fuel Moisture Content
FRI	Fluorescence Ratio Indices
GPR	Gaussian Process Regression
HIS	Hyperspectral image
HS	Hyperspectral
ISS	International Space Station
LAI	Leaf Area Index
LCC	Leaf Chlorophyll Content
LNC	Leaf Nitrogen Content
LST	Land surface temperature
LSTM	Copernicus Land Surface Temperature Monitoring
LSSVM	Least Square Support Vector Machine
LUT	Look-up Tables
LWC	Leaf Water Content
ML	Machine Learning
MODIS	Moderate Resolution Imaging Spectroradiometer
NDVI	Normalized Difference Vegetation Index
PCA	Principal Component Analysis
PLSR	Partial Least Squares Regression
PRI	Photochemical Reflectance Index
PRISMA	PRecursore IperSpettrale della Missione Applicativa
R&D	Research & Development
REIP	Red Edge Inflection Point

D03 - State-of-the-art review report on
the EO analysis method/s and
algorithm/s

RF	Random Forest
RGB	Red green blue
RMSE	Root mean squared error
RTM	Radiative transfer model
SEB	Surface energy balance
SiVM	Simplex Volume Maximisation
SNR	Signal-to-noise ratio
SST	Sea surface temperature
SVM	Support Vector Machine
SWIR	Short Wave Infrared
TCI	Temperature condition index
TES	Thermal emissivity spectra
TIR	Thermal infrared
TsHARP	Sharpening thermal imagery
TVDI	Temperature – Vegetation Dryness Index
TVMDI	Temperature-Vegetation-soil Moisture Dryness Index
UAV	Unmanned aerial vehicle
VCI	Vegetation condition index
VHI	Vegetation health index
VIIRS	Visible Infrared Imaging Radiometer Suite
VIS	Visible
VNIR	Visible and near-infrared
VPD	Vapor pressure deficit
VTCI	Vegetation Temperature Condition Index
WI	Water Index

D03 - State-of-the-art review report on
the EO analysis method/s and
algorithm/s

1 Thermal and Hyperspectral Data in ARIES

1.1 Introduction

EO AFRICA (African Framework for Research Innovation, Communities and Applications) is a research and development initiative by ESA. It focuses on building African-European R&D partnerships and the facilitation of the sustainable adoption of Earth Observation and related space technology in Africa.

Within "ARIES" experimental EO analysis techniques will be developed and validated, addressing water management and food security in Africa. Those techniques, algorithms and prototype solutions will be based on a new generation of upcoming operational EO data: thermal and hyperspectral. The utilization of hyperspectral (PRISMA) and thermal data (ECOSTRESS) will deliver important information for the design of future missions (CHIME, LSTM). Additionally, algorithms that can be used on such data and tools for its efficient processing will be developed. Doing this in an African setting means, that future services will take into account the needs of African users.

2 State-of-the-Art Thermal Data

2.1 Thermal Data – Characteristics

All objects with temperatures above absolute zero emit radiation. The wavelength of the emitted radiation depends on the temperature of the object, as prescribed by Wien's displacement law. With an average temperature of around 300 K, the Earth typically emits radiation in the 8-14 µm domain, a wavelength range captured by thermal sensors. Measurements of emitted radiation as captured by thermal sensors can be converted to temperature of the emitting surface using the Stefan-Boltzmann law, which states that the total amount of electromagnetic radiation emitted by a blackbody is directly related to its temperature. In the context of Earth observation, we talk about Land Surface Temperature (LST) or Sea Surface Temperature (SST), depending on the application. A blackbody is a hypothetical surface which emits all energy it absorbs. However, very few real objects behave like a perfect blackbody. The emissivity of a surface denotes the radiant flux of an object at a given temperature over the radiant flux of a blackbody at the same temperature. For thermal remote sensing, this means that the temperature measured at the sensor does not necessarily match the temperature of the objects on the Earth's surface. It is therefore important that the necessary emissivity corrections are done when deriving land surface temperature from thermal measurements.

D03 - State-of-the-art review report on
the EO analysis method/s and
algorithm/s

Thermal imaging is able to contribute to mapping and monitoring of vegetation, forest fires, geology, determination of soil and surface type, hydrothermal investigations, monitoring of volcanic, mineral, and natural hazards, sea surface temperature, ocean colour, and hydrology, among other applications. Given the specific focus of ARIES on regional water stress and drought monitoring, the remainder of this literature review will focus specifically on the role of satellite thermal infrared (TIR) data for vegetation monitoring. In this respect, thermal remote sensing has received relatively little attention as compared to optical (VIS/VNIR) remote sensing, simply due to the fact that the application of thermal remote sensing is very often challenged due to a lack of high spatio-temporal TIR datasets and contamination of data streams by clouds. Current TIR products are a compromise between high (low)-spatial and low(high)-temporal resolution. In the next section, we specifically focus on the potential of satellite thermal data for vegetation monitoring and discuss current approaches, limitations and opportunities.

2.2 Thermal Data for Water Stress and Vegetation Monitoring

2.2.1 Introduction

To ensure global water and food security, a timely identification of plant water stress or drought conditions is of utmost importance. Good knowledge of crop water status across expansive farming areas can optimize agricultural water use. Water stress (drought) leads to the physiological reactions by plants generated due to the shortage of plant available water. Such condition is encountered due to prolonged absence of precipitation, that leads to a unique condition of rising soil water deficit in conjunction with high evaporative demand from the atmosphere *(Mallick et al., 2018; 2022)*. Water stress is one of the most important abiotic stressors that limit plant development, crop yield, and food quality (*Jones & Schofield, 2008*). Before apparent indications of water stress show, plants might be irreparably damaged (*Mahajan & Tuteja, 2005*). Consequently, a pre-symptomatic or pre-visual identification of plant physiological changes might significantly aid in preventing severe crop losses.

Cell turgor and leaf water content are diminished under severe and/or persistent water stress (*Jones, 2004*). As a result, stomatal closure reduces the exchange of water vapor between plants and the atmosphere, reducing the evaporative cooling effect and resulting in an increase in plant surface temperature relative to a plant that is not under water stress (*Inoue et al.,1990*). Nonetheless, stomata regulate not just plant transpiration but also photosynthetic CO_2 uptake, which prevents CO_2 absorption and fixation. Due to stomatal closure, the photosynthetic rate is lowered, resulting in a decrease in yield. While a decrease in CO_2 uptake owing to stomatal closure reduces the photosynthetic rate, irradiance and absorbed photosynthetically active radiation (**fAPAR**) remain unchanged. It is well established, based on the leaf energy balance equation, that leaf temperature fluctuates with (evapo)transpiration rates of the leaves and is,

D03 - State-of-the-art review report on
the EO analysis method/s and
algorithm/s

thus, a function of stomatal conductance. Temperature of the leaf has an inverse relationship with transpiration rate. Typically, the leaf temperature of a fully transpiring plant is between 2 and 5 degrees Celsius below the ambient air temperature (*Jones, 1999*).

Aside from the clear conceptual link between water stress and leaf/canopy temperature, the latter can be related to other vegetation characteristics such as fractional vegetation cover. For example, under severe water stress, a full-grown canopy can exhibit elevated canopy temperature as compared to the unstressed vegetation with same vegetation cover. On the other hand, arid and semi-arid complex ecosystems with sparse vegetation cover tend to exhibit substantially higher canopy temperatures as compared to sparse vegetation in humid continental ecosystems.

In addition to LST, the land surface emissivity (LSE) is also considered to represent the ecohydrological characteristics of ecosystems. Arid and semi-arid ecosystems generally have large variations in transpiration (Hulley et al., 2015; Masiello et al., 2014) which is mostly associated with high coefficient of variation of soil water content, low ratio of transpiration to net available energy, and high potential evaporative demand with respect to precipitation. LSE of natural land surfaces is determined by soil geologic material, organic matter, moisture content, and vegetation-cover characteristics. However, LSE is independent from the soil temperature profile or temperature of the underlying surface. Since the thermal infrared radiance measured by satellite radiometers also contain the signals of both temperature and emissivity, LSE needs to be segregated from temperature (Jin and Liang, 2006). LSE is also a slow changing variable and offers little towards vegetation monitoring at large spatial scale.

As opposed to **VNIR/SWIR** spectra, which are primarily dominated by overtones and combination modes of fundamental vibrations resulting from interactions between solar radiation and leaf contents, **TIR** spectra are primarily derived from primary absorption bands of biochemical leaf compounds, such as cellulose, and should therefore exhibit higher spectral contrast (*Ribeiro da Luz, 2006*). Therefore, changes in the emissivity spectra should coincide with changes in the proportions of leaf elements brought on by water stress (*Ullah et al., 2013*).

2.2.2 Methods and Algorithms

Indicators based on land surface temperature

Since the 1970s, **TIR** remote sensing (8–14 μm) has been recognized as a "*possible*" method for early detection of plant water stress. The bulk of research estimate temperature-based indices for the identification of plant responses to water stress using broadband TIR sensors (*Zarco-Tejada et al., 2013*). The first attempt to convert leaf/canopy surface temperatures to a notion on crop water stress was done by subtracting ambient air temperature from the measured LST, where values larger than 0 point to stressed conditions (*Jackson et al.,1977;*

D03 - State-of-the-art review report on
the EO analysis method/s and
algorithm/s

Idso et al., 1977). The Crop Water Stress Index (**CWSI**) further exploited this idea and made it more applicable for remote sensing applications. CWSI is defined as:

$$CWSI = (T_{leaf} - T_{wet}) / (T_{dry} - T_{wet})$$

Where T_{wet} represents the leaf/canopy temperature of an optimally transpiring crop and T_{dry} represents a non-transpiring crop (*Jackson et al., 1981*). By using these theoretical upper and lower boundaries of transpiration, CWSI implicitly also accounts for other factors potentially affecting crop water stress, such as wind, radiation and vapor pressure deficit (**VPD**) and should be applicable for any crop and any environmental condition (*Gerhards et al., 2019*). One should note however that temperature differences between stressed and non-stressed plants can be very subtle in humid and/or cold climates due to low VPD and hence care should be taken when applying this approach in temperate climates.

Although originally designed to be applied on field measurements of leaf/canopy temperature, the concept of CWSI has been adopted to remotely determine crop water stress conditions based on LST derived from satellite data. From a remote sensing perspective, this requires good knowledge on which crop is planted where and the upper and lower temperature boundaries for each crop/land cover present in the scene. The latter can be derived through a field measurement campaign for the specific crop or land cover of interest, as was for instance done by *Ciezkowski et al. (2020)* to study crop water stress in wetlands using thermal UAV data. To overcome these specific data requirements, *Veysi et al. (2017)* proposed an adjusted version of CWSI which can be purely derived from satellite data, i.e., a combination of **LST** and the well-known Normalized Difference Vegetation Index (**NDVI**) derived from optical satellite data. In their definition, T_{wet} and T_{dry} are replaced by T_{cold} and T_{hot} signifying the coldest and hottest vegetated pixel within the image scene. Another way of minimizing the need for additional data is to rely on the standard deviation of canopy temperature (**CTSD**) as an indicator for water stress, as was successfully demonstrated for even moderately stressed crops (*González-Dugo et al., 2006*).

The combination of LST data and more generic data on crop condition as provided by the NDVI and similar metrics is a frequently used strategy in determining crop water stress and onset/occurrence of droughts through the use of remotely sensed data. One example is the Vegetation Health Index (**VHI**), being a linear combination of the Vegetation Condition Index (**VCI**, capturing temporal anomalies in NDVI) and the Temperature Condition Index (**TCI**, capturing temporal anomalies in canopy temperature), and used operationally at 1 km spatial resolution (AVHRR data) as basis for the Agricultural Stress Index system by FAO (*Van Hoolst et al., 2016*). Another example at low spatial resolution is the Temperature – Vegetation Dryness Index (**TVDI**), where an empirical relation was constructed between LST and NDVI, resulting in an index tightly linked to surface soil moisture (*Sandholt et al., 2002*). High resolution examples of the same concept include the Vegetation Temperature Condition Index

D03 - State-of-the-art review report on
the EO analysis method/s and
algorithm/s

(VTCI), as implemented by *Zhou et al. (2020)*, where they used MODIS LST and Sentinel-2 optical imagery to first derive a high-resolution estimate of LST (for more information, see next section) and subsequently compute the VTCI, as defined by:

$$\text{VTCI} = \frac{LST_{max}(NDVI_i) - LST(NDVI_i)}{LST_{max}(NDVI_i) - LST_{min}(NDVI_i)}$$

Where for each pixel, the NDVI value is used as a guideline to search for the most suited maximum and minimum LST boundaries to be applied. A more complex formulation has been suggested by *Amani et al. (2017),* who added a soil moisture component to their Temperature-Vegetation-soil Moisture Dryness Index (TVMDI) to estimate drought risk purely based on optical and thermal data from either Landsat 8 or MODIS.

Note that most of the indicators mentioned above provide a relative measure of crop water stress, which should be carefully interpreted by agronomic experts to translate these indicators to relevant information to farmers, e.g., on the recommended timing and amount of irrigation water to be applied. Indeed, further research is needed to determine crop type specific thresholds for these indicators (*Gerhards et al., 2019*).

In addition to the index-based approaches, time series information of LST, rainfall, fAPAR, and NDVI can also be used for vegetation health monitoring. For example, the intra-seasonal and inter-annual variability in LST and rainfall can be statistically linked with the intra-seasonal and inter-annual variability of NDVI and enhanced vegetation index (EVI). While *Kato et al. (2021)* assessed the inter-annual variability of vegetation phenological events using satellite vegetation index time series in drylands, *Brando et al. (2010)* assessed the seasonal and inter-annual variability of climate and vegetation indices across different sites in the Amazon Forest. This study showed that monthly EVI was positively correlated with PAR and that EVI variability was greatest in regions of water stress. *Yu et al. (2021)* (https://ieeexplore.ieee.org/document/9312390) reported interannual spatiotemporal variations of LST in China from 2003 to 2018. According to this study, significant changes in the annual mean LST were correlated with the change in vegetation coverage and the impact of land cover types on the interannual variations of LST is also determined in this study. No studies reported a comprehensive analysis on the possibility of vegetation monitoring by using the integrated information of LST, rainfall, fAPAR and multispectral satellite data information.

Use of land surface emissivity

A decent review on the use of LSE for vegetation monitoring is available in *Neinavaz et al. (2021).* According to the review, LSE spectra were found to be associated with fractional vegetation cover, which enables the detection of various types of land cover (*Hewison, 2001*). *Ribeiro da Luz and Crowley (2010)* identified nearly half of the fifty tree species using airborne

D03 - State-of-the-art review report on
the EO analysis method/s and
algorithm/s

hyperspectral TIR data with varying degrees of success. This study discussed the role of leaf angle distribution and leaf size and canopy structure on the LSE spectra contrast among species. *Meerdink et al. (2019)* demonstrated a significant difference between the canopy emissivity among different species using airborne hyperspectral TIR data. However, for most investigated species, the emissivity of the canopy was not representative of the emissivity of the leaves due to the influence of the canopy structure and leaf orientation. A few studies also reported the use of LST and LSE to retrieve biophysical and biochemical properties. *Banerjee et al. (2018)* demonstrated better accuracy of LAI retrieval in wheat using TIR data under different moisture stress conditions. A combination of LSE and spectral reflectance from VNIR and SWIR was found to improve the retrieval accuracy of LAI in a mixed temperate forest (*Neinavaz et al. 2019*). *Ullah et al (2012)* investigated the possibility of retrieving leaf water content using data from the mid- and long- water infrared regions. The fuel moisture content and equivalent water thickness as a proxy of vegetation water content could also be predicted at canopy level using hyperspectral TIR data. *Meerdink et al. (2016)* showed the integration of TIR data with VNIR/SWIR data could improve the prediction accuracy of foliar traits, including cellulose, lignin, leaf mass per area, nitrogen, and canopy water content.

From the emissivity based approach it can be said that: the generalization that vegetation does not generate sufficient spectral features in the **TIR** for studying plant physiological properties is contingent on a number of factors (*Ribeiro da Luz & Crowley, 2007*): (1) General lack of hyperspectral remote sensing instruments (most available setups are based on laboratory equipment); (2) Extremely low and complex spectrum emissivity fluctuations originate from intricate plant physiological and biochemical processes; (3) Airborne or satellite remote sensing **TIR** sensors with low signal-to-noise ratio (**SNR**) and low spatial and spectral resolution are incapable of detecting tiny fluctuations in the **TIR** spectral fingerprint of plants; (4) To extract precise emissivity spectra, atmospheric correction and advanced **TES** techniques are required.

Current **TIR** satellites do not meet the parameters (high **SNR**, high spectral and spatial resolution) necessary to measure the low spectral contrast emissivity characteristics of plants from space. Consequently, the scaling up of emissivity-based methods for detecting water stress from space is still somewhat limited. In order to better comprehend the relationships between the spectral emissivity characteristics and changes in leaf attributes under environmental stress situations at different remote sensing scales, additional fundamental study is required.

Modelling of evapotranspiration

The physically-based modeling of evapotranspiration (**ET**) could provide an alternative method not only for the detection of plant responses to water scarcity, but also for the elucidation of plant-soil-atmosphere interactions under environmental stress situations. Estimation of **ET** by

D03 - State-of-the-art review report on
the EO analysis method/s and
algorithm/s

TIR remote sensing is based on surface energy balance (**SEB**) models. The primary assumption of using land-surface temperature (**LST**) in a **SEB** model is, **TIR** remote sensing can provide direct information of the land-surface moisture status impacting the surface energy fluxes and their partitioning (*Norman et al., 1995*). Over time, many different ET models have been developed, e.g. SEBAL (*Bastiaanssen et al., 1998*), SSEBop (*Senay et al., 2013*), ALEXI/DisALEXI (*Anderson et al., 2011*), ETLook (*Bastiaanssen et al., 2012*), STIC (*Mallick et al., 2018; 2022; Trebs et al., 2021*), all showing slight differences in the way the problem is approached. While a full review of ET models is beyond the scope of this state-of-the-art review, the derived actual evapotranspiration can be used to estimate drought conditions and water stress levels. The Evaporative Stress index (ESI), computed as standardized anomalies of the ratio of actual to reference ET (*Anderson et al., 2007*). Whereas this ESI has been shown to well match other frequently used drought indicators when applied to low-resolution EO data at the continental scale (e.g. *Anderson et al., 2016*), different versions of this indicator are now being produced directly based on high resolution thermal data from ECOSTRESS, thereby increasing the potential of this indicator for precision agriculture applications.

2.2.3 Challenges and Future Developments

Numerous airborne and satellite **TIR** sensors have been created and utilized in agriculture due to the huge potential of temperature-based indices for the pre-visual identification of plant reactions to water stress (*Khanal et al., 2017*). As a result of their low spatial and/or temporal resolution, however, satellite sensors are inadequate for precision agriculture applications. Landsat 8 has the best spatial resolution with 100 m, which corresponds to a single field per pixel for the majority of agricultural cultivation systems (*Mahlein, 2016*). Consequently, recent advances in **TIR** remote sensing from airborne and Unmanned Aerial Vehicles (**UAV**s) offer the potential to bridge the gap between low-resolution satellite images and small-scale in situ measurements (*Berni et al., 2009*).

For highest benefit in agricultural water management applications, frequent thermal imaging (4-day revisit) at sub-field (100 m or less) spatial resolution is necessary. While the current fleet of Landsat satellites (7 and 8) provides the required spatial resolution, the 8-day combined revisit can be insufficient to detect quick changes in surface moisture status or crop phenology, especially in regions with persistent cloud cover. Current state-of-the-art thermal infrared sensing satellites deliver either high temporal (e.g., **MODIS**, **AVHRR**, **VIIRS**, or Sentinel-3 with 1–3 days revisit time) but coarse spatial (i.e., 1 km) resolution images or high spatial (e.g., Landsat series, Advanced Spaceborne Thermal Emission and Reflection Radiometer **(ASTER)** with 100 m) but low temporal (i.e., 16 days) resolution images. Multi-sensor scaling, such as pan-sharpening, or more advanced disaggregation techniques could be one solution (e.g., thermal sharpening or temperature unmixing). The combining of distinct spectral

D03 - State-of-the-art review report on
the EO analysis method/s and
algorithm/s

domains in a multi-sensor approach would provide the potential for novel soil–plant–atmosphere continuum discoveries (*Gerhards et al., 2019*).

The basic concept behind thermal sharpening is to model the relationship between the thermal and optical responses of the landscape at coarse spatial resolution and applying that model on high-resolution optical data to produce high-resolution thermal imagery. Traditionally, this relation is established with the shortwave-infrared reflectance bands of the optical sensor, as this information is tightly linked to water content, in turn an important explanatory factor for LST. TsHARP (sharpening thermal imagery), a widely used thermal sharpening technique, uses fractional vegetation cover (fc) derived from the NDVI as explanatory variable for the thermal behavior of the land surface (*Kustas et al., 2003; Agam et al., 2007*). A key assumption in TsHARP is that this relation between fc and LST remains constant throughout various landscapes, which has been shown by many subsequent studies to not be the case (e.g. *Jeganathan et al. 2011; Chen et al., 2012*). Through time, many adaptations to TsHARP have been suggested, including developing separate fc-LST relationships for different land cover types (Merlin et al., 2010) and adding additional explanatory variables such as albedo (*Dominguez et al., 2011*). All this research has demonstrated thermal sharpening should be done in a more flexible way. *Gao et al. (2012)* therefore introduced a data mining approach to thermal sharpening, where scene-specific regression trees are fitted between the thermal response and shortwave-infrared reflectance. This Data Mining Sharpener (DMS) clearly outperformed the traditional TsHARP technique, specifically in highly heterogeneous landscapes. DMS has later been adopted in the Sen-ET project, where it was used to produce sharpened LST based on Sentinel-3 thermal and Sentinel-2 optical data and in turn was combined with the two source energy balance (TSEB) model to generate 20m resolution ET estimates (*Guzinski et al., 2020*). Their implementation of the DMS has been released as open-source software on GitHub. A similar approach has been used by *Zhou et al. (2020)* to disaggregate MODIS LST data to the spatial resolution of Sentinel-2.

An important limitation of which users should be aware when combining satellite data from multiple platforms is the potential misalignment between products from different sensors due to differences in registration and orthorectification. *Xue et al. (2020)* for instance obtained a blurred result when sharpening ECOSTRESS data using Landsat optical imagery due to slight geometric shifts between both data sources. They therefore proposed a modified version of the DMS, extending the spatial window under consideration when identifying homogeneous low-resolution pixels in the thermal imagery, being an essential step during the sharpening procedure. They demonstrated this modification yielded more accurate results when combining thermal data from ECOSTRESS and VIIRS with harmonized Landsat-Sentinel data.

In the previous paragraph we have seen that the spatial resolution of thermal imagery can be improved through data fusion approaches with high-resolution optical imagery. Phenomena

D03 - State-of-the-art review report on
the EO analysis method/s and
algorithm/s

such as water stress and evapotranspiration are also highly dynamic in the temporal domain, implying that monitoring projects in the field of precision agriculture ideally require daily (or even sub-daily) LST observations. As different thermal sensors operate at different temporal frequencies and local overpass times, data from all these sensors could be combined to yield highly dense timeseries of LST and ET at field scale. One of the most recent efforts in this direction was performed by *Anderson et al. (2021)*, who evaluated the interoperability of Landsat and ECOSTRESS thermal data for producing ET image timeseries with high spatial (30 m) and temporal (daily) resolution. A data fusion algorithm was used to combine Landsat and ECOSTRESS ET retrievals at 30 m with daily 500-m retrievals utilizing TIR data from the Moderate Resolution Imaging Spectroradiometer (MODIS) sensor over agricultural sites of interest across the United States. The results highlighted the significance of the more frequent temporal sampling provided by ECOSTRESS, particularly in cloud-prone regions. The authors furthermore provide some practical guidelines with regard to ECOSTRESS data suitability (related to overpass time and viewing angles) for usage in this data fusion approach and stress the importance of simultaneous acquisition and availability of TIR and VSWIR reflectances in order to optimize ET retrieval based on these data. These first experiences should now be further tested in a range of different environmental conditions and properly validated to verify the robustness and transferability of the approach and underlying assumptions.

Due to the lack of multi- and hyperspectral TIR satellites and the current limitations with regards to spatial and temporal resolutions as outlined in the sections above, future thermal missions such as LSTM (Land-Surface Temperature Monitoring; *Koetz et al., 2019*) offer very promising perspectives for the use of multi-/hyperspectral TIR for the (early) detection of environmental stresses from space. The currently existing broadband **TIR** imagers (one spectral band in the wavebands of 8–14 µm) are based on the assumption of a constant emissivity, which does not exist in nature (e.g., 0.97 for vegetation; *Ullah et al., 2012*). Therefore, new hyperspectral **TIR** imagers offer new methodologies that enable exact spectral emissivity retrieval and, consequently, more accurate surface temperature calculation.

3   State-of-the-Art Hyperspectral Data

3.1   Hyperspectral Data – Characteristics

Hyperspectral (HS) data are characterized by their high range and bands of acquisition of the electromagnetic spectrum, compared to multispectral or RGB images. Typically, they cover the full spectrum between 400 and 2500 nm (VIS to SWIR) with hundreds of bands. E.g., the PRISMA sensor has 239 bands with a variable spectral bandwidth between 6 and 12 nm with a spatial resolution of 30 m.

D03 - State-of-the-art review report on
the EO analysis method/s and
algorithm/s

HS images (HSI) can be captured by e.g., push broom, filter wheel, and liquid crystal tuneable filters *(Fong and Wachman, 2008).* The incoming light is passing through a convex grating or a prism which separates the light into several wavelength by entering the respective line of the push broom sensor *(Lowe et al., 2017).* Compared to line-based push brooms, snapshot approaches capture an entire hyperspectral two-dimensional image at once, rather than just a line.

HSI allows for resolving physical, chemical, and biological components of the observed matter and therefore provides a kind of 'fingerprint' of the earth surface. Parameters and crucial information for agriculture, food security, soils, biodiversity, environmental degradation and hazards, inland and coastal waters, snow hydrology, and forestry can be derived from these fingerprints *(Rast and Painter, 2019).* HSI is a non-destructive method. Figure 1 illustrates the information retrieval from various surface materials, while Figure 2 shows the spectral signal of healthy and stressed vegetation on the hyperspectral range.

Starting in the early 1980s with airborne and end of the 1990s with spaceborne hyperspectral observations, it now has become one of the key research areas in remote sensing. The Italian PRecursore IperSpettrale della Missione Applicativa (PRISMA) is one of the first new generation spaceborne sensors, which was launched in March 2019 *(Loizzo et al., 2019).* PRISMA mission is aimed to acquire data for environmental monitoring such as agriculture *(Verrelst et al., 2021).* The hyperspectral push broom sensor has 239 bands ranging from 400 – 2 505 nm with a spectral resolution of 12 nm or higher. The satellite operates in a 615 km altitude sun-synchronous orbit with an inclination of 98.19°. The ground sampling distance is 30 m. The entire PRISMA mission is developed, owned, and controlled by the Italian Space Agency (ASI) and is set for five years (Loizzo et al., 2019).

Besides the already operating missions of PRISMA and the DLR`s DESIS on board of the ISS, several hyperspectral missions are being developed right now and planned to launch in the next years. For example, the ESA`s CHIME mission and the Chinese AHSI mission. Since the end of 2022, the German Environmental Mapping and Analysis Program (EnMAP) with a dual-spectrometer in the range between 420 and 2450 nm with a spectral bandwidth between 5 and 12 nm, a signal-to-noise ratio of 400:1 in the VIS-NIR and 180:1 in the SWIR bands provides data. The ground sampling distance of EnMAP is 30 m *(Guanter et al., 2015).*

D03 - State-of-the-art review report on
the EO analysis method/s and
algorithm/s
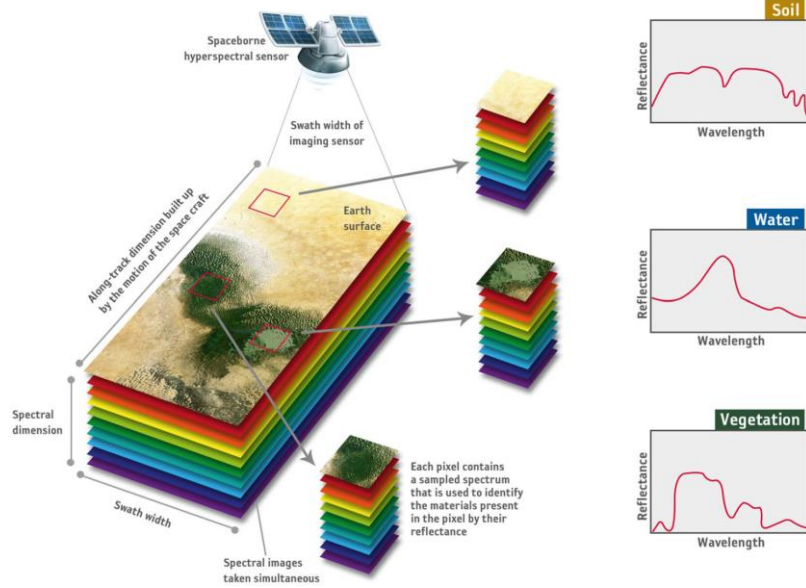
Figure 1: Imaging spectroscopy – principle of observation (ESA Earth Observation Graphic Bureau, in Rast und Painter (2019).
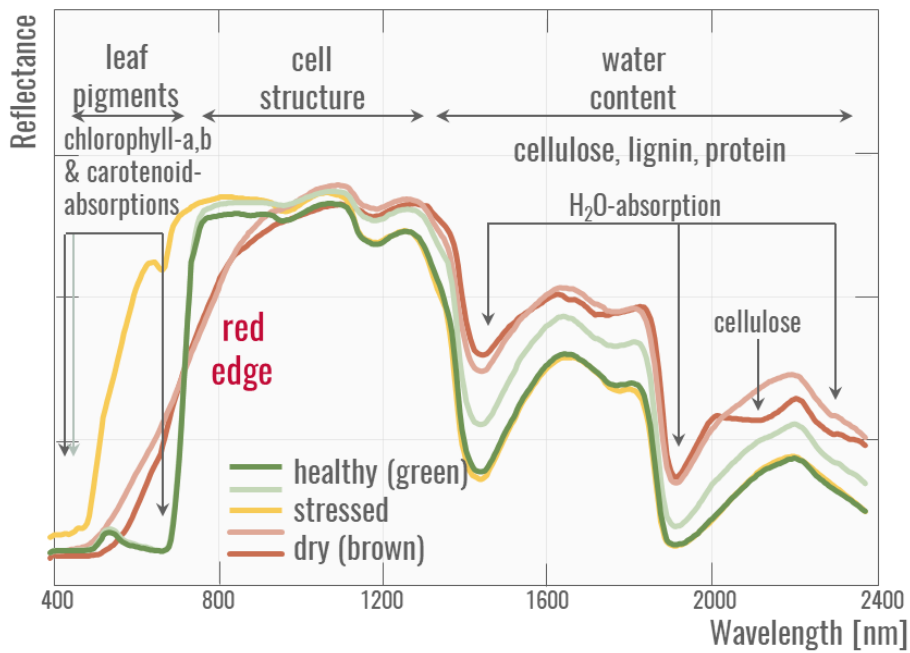
Figure 2: Hyperspectral range of healthy and stressed plants (Berger et al. 2020).

D03 - State-of-the-art review report on
the EO analysis method/s and
algorithm/s

3.2 Hyperspectral Data for Water Stress and Vegetation Monitoring

Since the main aim is to develop, implement, and validate algorithms and new EO data products addressing the water resource management using hyperspectral PRISMA data, state-of-the-art methods and products are reviewed and summarized in the following:

Leaf water content (LWC) and canopy water content (CWC) are vital parameters to monitor the plant development, water status, and a balanced water supply and irrigation. Water stored in agricultural plants is linked to biochemical factors such as vegetation transpiration *(Running et al., 1991)* and net primary production. Especially for agricultural management in arid regions, accurate retrieval of the water content and vegetation traits might be crucial for mitigating water stress due to climate-related droughts and heat-waves *(Tagliabue et al., 2022)*. The plant water content on leaf and canopy level (LWC/CWC) can be estimated from hyperspectral remote sensing data due to high absorptions of solar radiation by liquid water in the NIR (720–1 000 nm) and SWIR (1 000–2 500 nm). A key parameter is the leaf equivalent water thickness (EWT) [gcm^{-2}], defined as the quantity of liquid water per area of the leaf. The CWC is analogously defined as the quantity of liquid water per unit area of the ground surface [gm^{-2}]. Around 970 nm, 1 200 nm, 1 450 nm, 1 530 nm, 1 720 nm, 1 940 nm, and 2 500 nm the absorption is highest, as these wavelengths are the water absorption features. *Pu et al. (2003)* achieved good results in LWC estimation with indices in the 1 200 nm area based on the continuum removal technique, which takes into account relative local patterns of the spectrum.

By using physical-based radiative transfer models (RTM), the complex interactions between solar radiation and vegetation in the canopy layer can be described by simulated spectra with certain boundary parameters. Inversion of remote sensing acquired hyperspectral data allows the statistically estimation of canopy parameters using e.g., look-up tables (LUT) or machine learning (*Verhoef & Bach, 2007)*. Nevertheless, the ill-posed problem by different vegetation traits leading to equal spectral signals of the canopy is a disadvantage of common RTM inversion approaches. On the other hand, RTMs are able to consider observation angles and the spectral response functions of the specific bands within its simulation as well as to anticipate future satellite data by simulations (*Verhoef & Bach, 2012)*. Also, different crop types can be taken into account to simulate near-realistic spectra considering certain bio-chemical processes or plant stock geometries.

Besides the index-based approach, various studies achieved good results using a spectrum matching technique (e.g., MODTRAN-based RTM ACRON) to estimate water vapor and liquid water *(Trombetti et al., 2008)*. Originally developed to improve the AVIRIS water vapor

D03 - State-of-the-art review report on
the EO analysis method/s and
algorithm/s

retrieval, the commercial ACORN model fits the measured radiance at 940 nm to an ACORN-modeled radiance spectrum of the water vapor. Based on the Beer-Lambert Law, a simultaneous retrieval of liquid water and water vapor is possible due to spectral differences in the absorption maxima of the two *(Green et al., 1993; Cheng et al., 2006)*. *Champagne et al. (2003)* achieved good sensitivity to EWT and CWC for most crops but crops with dense stems such as corn. Especially during the early stages of plant growth of wheat, only poor results were obtained for within-crop EWT.

Several studies focused on the estimation of canopy water content using an index-based approach, such as the 970 nm water index (WI) developed by *Penuelas (2003)* for retrieval of relative plant water concentration *(Clevers, 2008; Vohland, 2008; Clevers, 2010, Cernicharo, 2013)*. On the canopy level it is proposed to use weak liquid water absorption bands around 850–860 nm, 970 nm, and 1 240 nm. This is caused by greater penetration of radiation within the canopy and lower saturation at the weaker water absorption bands at these wavelengths, especially for a high vegetation cover *(Behrens et al., 2006; Sims & Gamon, 2003; Sonnenschein et al., 2005)*. The WI overcomes the problem of saturated signals at high water contents and atmospheric water vapour due to strong absorptions by water in the 1450 nm and 1900 nm bands. However, the WI lacks generality, since different local boundary conditions may influence the WI significantly. Thus, it is proposed to use more spectral information of hyperspectral image data being available in the recent years (*Wocher et al., 2018)*.

Besides monitoring of the plant water content, early notice of plant stress due to a shortage of the water supply is very important. Water stress increases with the evaporative loss of water and limited soil water supply, which leads to a degradation of the physiological processes and lower yields of the plants.

Lowe et al. (2017) reviewed HSI analysis techniques for the detection and classification of the early onset of plant disease and stress. The following studies aimed to detect water stress and plant drought:

Thurau et al. (2010) identified water stress or crop drought before vegetation indices or visible detection by experts were possible. The simplex volume maximisation (SiVM) method was applied, which is a data clustering technique by using references of healthy and stressed spectra. *Römer et al. (2012)* analysed drought stress in barley and corn with SiVM. In-situ HS data between 470–750 nm was utilized after pre-processing with k-means clustering for reducing and filtering valid pixels and background signals. Compared to vegetation indices NDVI, PRI, REIP, and CRI, the SiVM approach detected partial water stress four days earlier. Another study of *Behmann et al. (2014)* applied the ML method of support vector machine (SVM) for learning drought or healthy plants during training with labelled ground truth data.

D03 - State-of-the-art review report on
the EO analysis method/s and
algorithm/s

Also, k-means clustering was used for pre-processing the HS data between 430–890 nm. While the approach of *Behmann et al. (2014)* detected drought stress on day 6, the NDVI was not able to detect it before day 16.

Least squares SVM (LSSVM) were applied by *Moshou et al. (2014)* to detect drought stress in wheat plants. In contrast to the aforementioned studies, they combined spectral reflectance and fluorescence data of six selected wavelength from a glasshouse study site. An accuracy of more than 99% was achieved for the classification in stressed and healthy plants.

Dobrowsky et al. (2005) calculated fluorescence ratio indices (FRI) for detecting plant heat and water stress. Wavelength affected by fluorescence such as 650–770 nm with emission peaks at 690 nm and 740 nm were used and normalized by non-affected wavelength like 600 nm and 800 nm.

Finally, *Kersting et al. (2012)* designed a Dirichlet aggregation regression (DAR) for barley drought stress prediction, that does not need any special HSI pre-processing technique and uses full HIS data dimensionality.

3.2.1 Method/s and Algorithms

Tagliabue et al. (2022) used PRISMA hyperspectral data for crop trait mapping over an agricultural area in north-east Italy between 2020 and 2021. By applying the PROSAIL-PRO radiative transfer model composition coupled with a Gaussian process regression algorithm, the crop traits leaf chlorophyll content (LCC), leaf nitrogen content (LNC), leaf water content (LWC), and corresponding parameters of the canopy level (CCC, CNC, and CWC) were estimated. Scaling to the canopy level was performed by the leaf area index (LAI). Validation with ground-truth data of 2020 revealed a good performance of $r^2 = 0.87$ for LNC, $r^2 = 0.67$ for LCC, $r^2 = 0.63$ for LWC for the leave level and slightly better performance for the canopy level: $r^2 = 0.92$ for CNC, $r^2 = 0.82$ for CCC, and $r^2 = 0.61$ for CWC.

The algorithm used by *Tagliabue et al. (2022)* is based on the simulation of 1 000 canopy reflectance spectra with the PROSAIL-PRO-4SAIL RTM. By applying principal component analysis (PCA), the dimensionality of the hyperspectral data was reduced and the best 15 principal components were used as approximation to the original simulated spectra. The resulting reduced dataset of simulated spectra was then used for training of a Gaussian process regression (GPR) machine learning model to predict LCC, LNC, and LWC plant traits maps based on a LUT between 1 000 simulated spectra and the plant trait parameters. Figure 3 summarizes the methodological approach of *Tagliabue et al. (2022)*.

D03 - State-of-the-art review report on
the EO analysis method/s and
algorithm/s
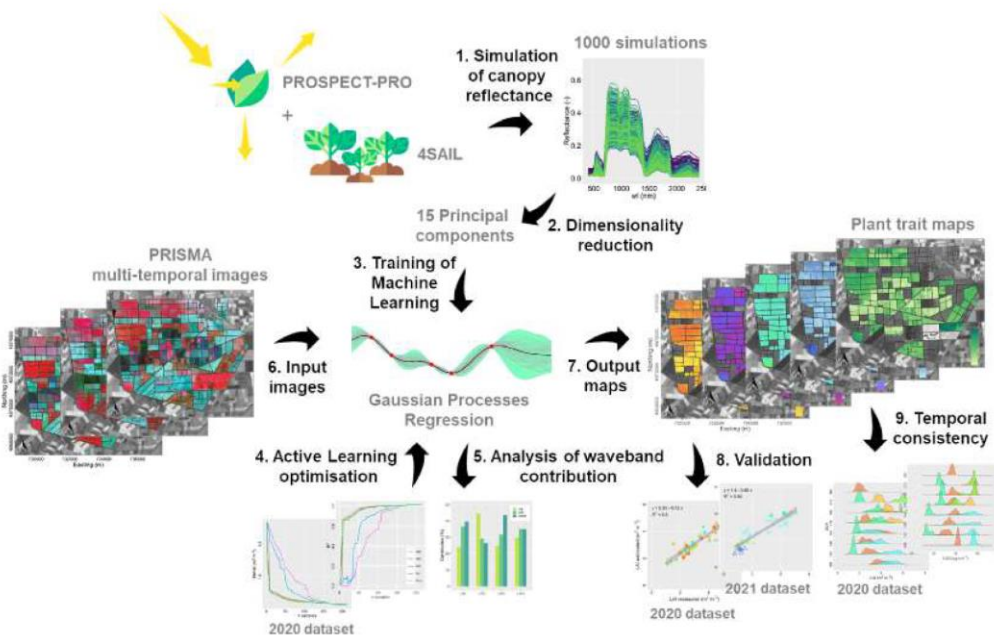
Figure 3: Flowchart summarizing the main steps of the plant trait retrieval workflow (Tagliabue et al. (2022).

The study area of *Tagliabue et al. (2022)* covered 3 850 ha in the town of Jolanda di Savoia in north-east Italy with fields of durum and soft wheat, barley, corn, sugar beet, alfalfa, soybean, rice, and medicinal plants. Field measurements were carried out for ground truth data.

The PRISMA satellite data in HDF5 format covering an entire phenological cycle were downloaded and pre-processed using the *prismaread, pracma*, and *FieldSpectroscopyCC* toolbox in R, designed by *Busetto and Ranghetti (2020), Borchers (2015)*, and *Wutzler et al. (2016)* in order to remove artefacts and compute smooth spectra. Regions of atmospheric water absorption between 1 350–1 510 nm and 1 795–2 000 nm, as well as the last bands of the SWIR (2 320–2 500 nm) were finally removed.

A study of *Elsherbiny et al. (2021)* focused on the feature selection and model development for CWC prediction. HS feature selection by vegetation indices, model-based features, and PCA were investigated using artificial neural networks (ANN), random forest (RF), and partial least square regression (PLSR). 128 HS images of rice crops under various laboratory-controlled water stress levels were in-situ taken by a NIR hyperspectral imaging system. The authors found robust feature selections by model-based features and PCA with most information provided by the 1 467, 1 456, and 1 106 nm bands for CWC prediction.

Also, *Yu et al. (2017)* predicted CWC based on remote HSI and RTM inversion. They used an UAV for data collection rather than a satellite and found that the range 900–1 100 nm mostly affected the CWC prediction.

D03 - State-of-the-art review report on
the EO analysis method/s and
algorithm/s

Wocher et al. (2018) developed a physical-based retrieval approach of canopy equivalent water thickness (EWT-C) using in-situ hyperspectral data. EWT-C was calculated based on the EWT of the leaves, stalks, and fruits, respectively. Based on the Beer-Lambert law, water content is inversely determined from the 930–1 060 nm spectral range of the canopy reflectance. Winter wheat and corn spectra from 2015, 2017, and 2018 of a test site in the north of Munich, Germany were used. For model calibration, 50 000 PROSPECT-D and PROSAIL spectra with corresponding LUT were applied. Validation was performed on in-situ measurements of water content of leaves, stalks, and fruits, while a correlation between measured and modeled data of up to R^2=0.72 for wheat and R^2=0.86 for corn were achieved. For wheat, the leaves and ears contained most information, while most reliable predictions of corn were only based on the leaf fraction.

Li et al. (2021) estimated EWT and fuel moisture content (FMC [%]) by new proposed spectral absorption indices SAI_{970}, SAI_{1200}, and SAI_{1660}. SAIs are calculated between two absorption shoulders as the ratio of an interpolated non-absorption and the measured absorption peak (relative absorption depth). These indices were developed to overcome the lack of considering specific plant species in most other studies and indices by using individual absorption peaks rather than fixed wavelength. They consider the symmetry of the absorptions at 970 nm, 1 200 nm, and 1 660 nm as well as the spectral heterogeneity of different leaves. For a study area in the Sichuan Province, China three species of trees were observed. Compared to other indices, a linear regression with the SAI_{1200} to EWT resulted in an optimal cross-validated R^2 of 0.845. The RATIO index achieved comparable performance. It was also found that the EWT was not significantly species specific, as the performance was weaker for the individual species than for a pooled dataset.

Verrelst et al. (2021) first used PRISMA data for canopy nitrogen content (CNC) retrieval with a hybrid RTM and machine learning model such as *Tagliabue et al. (2022)*. Synthetic simulated spectra of the PROSPECT-PRO and SAIL RTM were used as training dataset after dimensionality reduction using PCA. Active learning (AL) was used to optimize the training dataset for a GPR machine learning model. Also, non-vegetated spectra were added to the training dataset for better generalisation on heterogeneous spectral images. Validation on field measurements revealed an accuracy with an RMSE of 3.4 gm^{-2} and R^2 of 0.7.

Gerhards et al. (2016) conducted an experiment on 60 potato plants using broadband and hyperspectral thermal cameras as well as VNIR/SWIR spectroscopy. Water stress was found in the data before visual detection by indices and it was shown that pre-visual water stress detection was feasible using indices depicting leaf temperature, leaf water content, and spectral emissivity.

D03 - State-of-the-art review report on
the EO analysis method/s and
algorithm/s

Another review of HSI technologies and application in agriculture is given by *Lu et al. (2020)*. *Ahmad et al. (2021)* provide a review of the crop water stress assessment using remote sensing data.

3.2.1 Challenges and Future Developments

Based on the state-of-the-art literature discussed above, specific challenges and future developments arise on the application of hyperspectral data for the water stress and vegetation monitoring. While HS applications are under intense investigation, the algorithms range from narrowband spectral indices to physically-based ones coupled with RTM.

Using the capability of detecting narrow-band absorptions, HS applications offer the possibility of going one step further in terms of quantitative analyses. This gives a boost to both physically-based analysis methods, that can integrate causes and offer explanations for the detected crop values, as well as opening up new possibilities for deep learning and machine learning approaches due to the data depth of HS acquisitions. Nevertheless, AI algorithms require large amounts of data covering several land surfaces and long time-series for training. Currently, no such datasets are available from satellite, and mostly field studies and airborne data are utilized for algorithm development, which by the nature of these expensive campaigns, limits both the spatial and temporal availability of the HS data.

PRISMA and EnMAP are now a first step to providing longer time series from satellites and can be used in preparation for future missions like ESA's CHIME, which will open up the potential for operational HS applications in agriculture.

4 Conclusion

4.1 Thermal Algorithms

From the literature review presented in this document, we can conclude that many specific indicators and approaches have already been suggested to derive information on crop water stress from LST data at various spatial resolutions, all having clearly demonstrated the added value of thermal observations in the context of agricultural drought monitoring. The main challenges that remain are threefold, indicating the main research activities within ARIES to be performed regarding thermal data processing:

- The low spatial and temporal resolutions of current platforms do not allow for the detailed monitoring crop water stress at individual field scale, limiting applications of thermal data in the context of precision agriculture. While waiting for new platforms to be launched, more research should be devoted towards combining thermal and optical data acquired from different platforms to yield daily LST timeseries at high spatial

D03 - State-of-the-art review report on
the EO analysis method/s and
algorithm/s

resolution. Hence, within ARIES we specifically aim to test thermal sharpening and LST data fusion in the context of African agricultural systems.

- The translation of crop water stress indicators into more comprehensive indicators on drought onset, drought severity and drought impact on crop/biomass production remains a challenging task, as this requires some additional information on e.g., crop type and precipitation. Within ARIES, we aim to further investigate how a thermal crop water stress indicator can be used to infer this type of information in a timely manner. One way this problem can be approached, is by linking intra-seasonal LST anomalies with biomass productivity anomalies. One should note however that this can only be accomplished in case sufficient in-situ data on biomass production can be acquired from the African Early Adopters.

- In addition to these two above mentioned challenges, ARIES will also investigate the synergistic use of TIR and shortwave infrared reflectance information to develop a hybrid water stress indicator. Such approach will not only mitigate the shortcoming of TIR but also open up avenues towards the application of sensor synergy by using water sensitive information from satellite sensors.

4.2 Hyperspectral Algorithms

From the above literature review it becomes clear that HS applications are under intense investigation, the existing algorithms range from narrowband spectral indices to physically-based ones coupled with RTM. Much of the work so far relies on field studies and airborne data. While these types of data are of great value for the development of algorithms and for the exploration of the potential of HS data for the detection of crop water stress, they will not lead to actual applications in the sense that they are applicable to a diversity of places and situations, simply because they lack spatial and temporal availability. The longer times series from PRISMA and EnMAP will open up the potential for operational HS applications in agriculture. Exploring this potential in diverse African agricultural and pastoral settings, ARIES will examine the performance of selected existing algorithms and aims adjust them accordingly or come up with altogether new solutions, as required to meet the needs of our African users.

D03 - State-of-the-art review report on
the EO analysis method/s and
algorithm/s

5   References

Bibliography Thermal

Agam, N.; Kustas, W.P.; Anderson, M.C.; Li, F.; Neale, C.M.U. (2007). A vegetation index based technique for spatial sharpening of thermal imagery. Remote Sens. Environ., 107, 545–558.

Anderson, M.C., Norman, J.M., Mecikalski, J.R., Otkin, J.A., & Kustas, W.P. (2007). A climatological study of evapotranspiration and moisture stress across the continental U.S. based on thermal remote sensing: II. Surface moisture climatology. J. Geophys. Res., 112, D11112.

Anderson, M. C., Kustas, W.P., Norman, J.M., Hain, C.R., Mecikalski, J.R., Schultz, L., González-Dugo, M.P., Cammalleri, C., d'Urso, G., Pimstein, A., Gao, F. (2011). Mapping daily evapotranspiration at field to continental scales using geostationary and polar orbiting satellite imagery. Hydrology and Earth System Sciences, 15(1).

Anderson, M.C., Zolin, C., Sentelhas, P.C., Hain, C.R., Semmens, K.A., Yilmaz, M.T., Gao, F., Otkin, J.A., & Tetrault, R. (2016). The Evaporative Stress Index as an indicator of agricultural drought in Brazil: An assessment based on crop yield impacts. Remote Sens. Environ., 174, 82-99.

Anderson, M. C., Yang, Y., Xue, J., Knipper, K. R., Yang, Y., Gao, F., Hain, C. R., Kustas, W.P., Cawse-Nicholson, K., Hulley, G., Fisher, J. B., Alfieri, J.G., Meyers, T. P., Prueger, J., Baldocchi, D.D., Rey-Sanchez, C. (2021). Interoperability of ECOSTRESS and Landsat for mapping evapotranspiration time series at sub-field scales. Remote Sensing of Environment, 252 (112189).

Bastiaanssen, W.G.M., Menenti, M., Feddes, R.A., Holtslag, A.A.M. (1998). A remote sensing surface energy balance algorithm for land (SEBAL). 1. Formulation. Journal of Hydrology, 212-213, 198-212.

Bastiaanssen, W.G.M., Cheema, M.J.M., Immerzeel, W.W., Miltenburg, I.J., Pelgrum, H. (2012). Surface energy balance and actual evapotranspiration of the transboundary Indus Basin estimated from satellite measurements and the ETLook model. Water Resources Research.

Berni, J.; Zarco-Tejada, P.J.; Suarez, L.; Fereres, E. (2009). Thermal and Narrowband Multispectral Remote Sensing for Vegetation Monitoring From an Unmanned Aerial Vehicle. IEEE Trans. Geosci. Remote Sens., 47, 722–738.

Chen, X.; Yamaguchi, Y.; Chen, J.; Shi, Y. (2012). Scale effect of vegetation-index-based spatial sharpening for thermal imagery: A simulation study by ASTER data. IEEE Geosci. Remote Sens. Lett., 9, 549–553.

Ciezkowski, W., Szporak-Wasilewska, S., Kleniewska, M., Jóźwiak, J., Gnatowski, T., Dabrowski, P., Góraj, M., SzatyLowicz, J., Ignar, S., Chormański, J., (2020). Remotely sensed land surface temperature-based water stress index for wetland habitats. Remote Sensing, 12(4).

Dominguez, A.; Kleissl, J.; Luvall, J.C.; Rickman, D.L. (2011). High-resolution urban thermal sharpener (HUTS). Remote Sens. Environ., 115, 1772–1780.

Fisher, J. B., Tu, K., Baldocchi D.D. (2008). Global estimates of the land-atmosphere water flux based on monthly AVHRR and ISLSCP-II data, validated at 16 FLUXNET sites, Remote Sensing of Environment, 112(3), 901-919.

D03 - State-of-the-art review report on
the EO analysis method/s and
algorithm/s

Gao, F., Kustas, W.P., Anderson, M.C., (2012). A data mining approach for sharpening thermal satellite imagery over land. Remote Sens. 4, 3287–3319.

Gerhards, M., Schlerf, M., Mallick, K., Udelhoven, T., (2019). Challenges and Future Perspectives of Multi-/Hyperspectral Thermal Infrared Remote Sensing for Crop Water-Stress Detection: A Review. Remote Sens., 11, 1240.

González-Dugo, M., Moran, M., Mateos, L., Bryant, R. (2006). Canopy temperature variability as an indicator of crop water stress severity. Irrig. Sci., 24, p. 233.

Guzinski, R., Nieto, H., Sandholt, I., Karamitillios, G., (2020), Modelling High-Resolution Actual Evapotranspiration through Sentinel-2 and Sentinel-3 Data Fusion, Remote Sens., 12(9).

Hu, T., Mallick, K., Hulley, G., Perez, L., Frank, M., Schlerf, M., Hitzelberger, P., Didry, Y., Szantoi, Z., Alonso, I., Hook, S., (2022), Continental-scale evaluation of three ECOSTRESS land surface temperature products over Europe and Africa: Temperature-based validation and cross-satellite comparison. Remote Sensing of Environment, 282(113296).

Hulley, G. C., S. J. Hook, E. Abbott,N. Malakar, T. Islam, and M. Abrams (2015), The ASTER Global EmissivityDataset (ASTER GED): Mapping Earth'semissivity at 100 meter spatial scale,Geophys. Res. Lett.,42, 7966–7976,doi:10.1002/2015GL065564.

Idso, S.B.; Jackson, R.D.; Reginato, R.J. (1977). Remote-Sensing of Crop Yields. Science, 196, 19–25.

Inoue, Y.; Kimball, B.A.; Jackson, R.D.; Pinter, P.J.; Reginato, R.J. (1990). Remote estimation of leaf transpiration rate and stomatal resistance based on infrared thermometry. Agric. For. Meteorol., 51, 21–33.

Jackson, R.D.; Reginato, R.J.; Idso, S.B. (1977). Wheat canopy temperature: A practical tool for evaluating water requirements. Water Resour. Res., 13, 651–656.

Jackson, R.D.; Idso, S.B.; Reginato, R.J.; Pinter, P.J. (1981). Canopy temperature as a crop water stress indicator. Water Resour. Res., 17, 1133–1138.

Jeganathan, C.; Hamm, N.A.S.; Mukherjee, S.; Atkinson, P.M.; Raju, P.L.N.; Dadhwal, V.K. (2011). Evaluating a thermal image sharpening model over a mixed agricultural landscape in India. Int. J. Appl. Earth Obs., 13, 178–191.

Jin, M., & Liang, S. (2006). An Improved Land Surface Emissivity Parameter for Land Surface Models Using Global Remote Sensing Observations, Journal of Climate, 19(12), 2867-2881. Retrieved Feb 7, 2023, from https://journals.ametsoc.org/view/journals/clim/19/12/jcli3720.1.xml

Jones, H.G. (1999). Use of thermography for quantitative studies of spatial and temporal variation of stomatal conductance over leaf surfaces. Plant Cell Environ., 22, 1043–1055.

Jones, H.G. (2004). Application of Thermal Imaging and Infrared Sensing in Plant Physiology and Ecophysiology. In Advances in Botanical Research; Callow, J.A., Ed.; Elsevier Academic Press: San Diego, CA, USA; London, UK, 2004; Volume 41, pp. 107–163.

Jones, H.G.; Schofield, P. (2008). Thermal and other remote sensing of plant stress. Gen. Appl. Plant Physiol. 2008, 34, 19–32.

Khanal, S.; Fulton, J.; Shearer, S. (2017). An overview of current and potential applications of thermal remote sensing in precision agriculture. Comput. Electron. Agric., 139, 22–32.

D03 - State-of-the-art review report on
the EO analysis method/s and
algorithm/s

Koetz, B.; Berger, M.; Blommaert, J.; Del Bello, U.; Drusch, M.; Duca, R.; Gascon, F.; Ghent, D.; Hoogeveen, J.; Hook, S.; et al. (2019). Copernicus High Spatio-Temporal Resolution Land Surface Temperature Mission: Mission Requirements Document. Available online: http://esamultimedia.esa.int/docs/EarthObservation/Copernicus_LSTM_MRD_v2.0_Issued20190308.pdf

Kustas, W.P.; Norman, J.M.; Anderson, M.C.; French, A.N. (2003). Estimating subpixel surface temperatures and energy fluxes from the vegetation index-radiometric temperature relationship. Remote Sens. Environ., 85, 429–440.

Mahajan, S.; Tuteja, N. (2005). Cold, salinity and drought stresses: An overview. Arch. Biochem. Biophys., 444, 139–158.

Mahlein, A.-K. (2016). Present and Future Trends in Plant Disease Detection. Plant Dis., 100, 1–11.

Mallick, K., Toivonen, E., Trebs, I., Boegh, E., Cleverly, J., Eamus, D., Koivusalo, H., Drewry, D., Arndt, S.K., Griebel, A., Beringer, J., Garcia, M. (2018). Bridging Thermal Infrared Sensing and Physically-Based Evapotranspiration Modeling: From Theoretical Implementation to Validation Across an Aridity Gradient in Australian Ecosystems. Water Resources Research, 54(5), 3409-3435.

Mallick, K., Baldocchi, D., Jarvis, A. et al. (2022). Insights Into the Aerodynamic Versus Radiometric Surface Temperature Debate in Thermal-Based Evaporation Modeling. Geophysical Research Letters, 49(15).

Merlin, O.; Duchemin, B.; Hagolle, O.; Jacob, F.; Coudert, B.; Chehbouni, G.; Dedieu, G.; Garatuza, J.; Kerr, Y. (2010). Disaggregation of MODIS surface temperature over an agricultural area using a time series of Formosat-2 images. Remote Sens. Environ., 114, 2500–2512.

Neinavaz, E., Schlerf, M., Darvishzadeh, R., Gerhards, M., Skidmore, A.K. (2021). Thermal infrared remote sensing of vegetation: Current status and perspectives. International Journal of Applied Earth Observation and Geoinformation, 102, 102415.

Norman, J.M.; Kustas,W.P.; Humes, K.S. (1995). Source approach for estimating soil and vegetation energy fluxes in observations of directional radiometric surface temperature. Agric. For. Meteorol., 77, 263–293.

Ribeiro da Luz, B. (2006). Attenuated total reflectance spectroscopy of plant leaves: a tool for ecological and botanical studies. New Phytol., 172, 305–318.

Ribeiro da Luz, B.; Crowley, J.K. (2007). Spectral reflectance and emissivity features of broad leaf plants: Prospects for remote sensing in the thermal infrared (8.0–14.0 μm). Remote Sens. Environ., 109, 393–405.

Sandholt, I., Rasmussen, K., Andersen, J. (2002). A simple interpretation of the surface temperature/vegetation index space for assessment of surface moisture status. Remote Sens. Environ., 79 (2), pp. 213-224.

Senay, G.B., Bohms, S., Singh, R.K., Gowda, P.H., Velpuri, N.M., Alemu, H., Verdin, J.P. (2013). Operational Evapotranspiration Mapping Using Remote Sensing and Weather Datasets: A New Parameterization for the SSEB Approach. Journal of the American Water Resources Association.

Ullah, S.; Schlerf, M.; Skidmore, A.K.; Hecker, C. (2012). Identifying plant species using mid-wave infrared (2.5–6 μm) and thermal infrared (8–14 μm) emissivity spectra. Remote Sens. Environ., 118, 95–102.

D03 - State-of-the-art review report on
the EO analysis method/s and
algorithm/s

Ullah, S.; Skidmore, A.K.; Groen, T.A.; Schlerf, M. (2013). Evaluation of three proposed indices for the retrieval of leaf water content from the mid-wave infrared (2–6m) spectra. Agric. For. Meteorol., 171–172, 65–71.

Van Hoolst, R., Eerens, H., Haesen, D., Royer, A., Bydekerke, L., Rojas, O., Li, Y., Racionzer, P. (2016). FAO's AVHRR-based Agricultural Stress Index System (ASIS) for global drought monitoring. International Journal of Remote Sensing. 37. 418-439.

Veysi, S., Naseri, A.A., Hamzeh, S., Bartholomeus, H., (2017). A satellite-based crop water stress index for irrigation scheduling in sugarcane fields, Agricultural Water Management, 189, 70–86.

Xue, J., Anderson, M.C., Gao, F., Hain, C., Sun, L., Yang, Y., Knipper, K.R., Kustas, W.P., Torres-Rua, A., Schull, M.A., (2020). Sharpening ECOSTRESS and VIIRS land surface temperature using harmonized Landsat-sentinel surface reflectance. Remote Sens. Environ. 251, 112055.

Zarco-Tejada, P.J.; González-Dugo, V.; Williams, L.E.; Suárez, L.; Berni, J.A.J.; Goldhamer, D.; Fereres, E. (2013). A PRI-based water stress index combining structural and chlorophyll effects: Assessment using diurnal narrow-band airborne imagery and the CWSI thermal index. Remote Sens. Environ., 138, 38–50.

Zhou, X., Wang, P., Tansey, K., Zhang, S., Li, H., Wang, L. (2020). Developing a fused vegetation temperature condition index for drought monitoring at field scales using Sentinel-2 and MODIS imagery. Computers and Electronics in Agriculture,168,105144.

Bibliography Hyperspectral

Ahmad, U., Alvino, A., & Marino, S. (2021). A Review of Crop Water Stress Assessment Using Remote Sensing. *Remote Sensing*, *13*, 4155. https://doi.org/10.3390/rs13204155

Banerjee, K., Krishnan, P., Mridha, N., 2018. Application of thermal imaging of wheat crop canopy to estimate leaf area index under different moisture stress conditions. Biosyst. Eng. 166, 13–27.

Behmann J, Steinrücken J, Plümer L. (2014). Detection of early plant stress responses in hyperspectral images. ISPRS J Photogramm Remote Sens. 93:98–111.

Behrens, T., Müller, J.& Diepenbrock, W. (2006). Utilization of canopy reflectance to predict properties of oilseed rape (Brassica napus L.) and barley (Hordeum vulgare L.) during ontogenesis. European Journal of Agronomy, 25, 345–355.

Borchers, H., 2015. Pracma: practical numerical math functions.

Brando, P., et al. (2010), Seasonal and interannual variability of climate and vegetation indices across the Amazon, PNAS, 107 (33) 14685-14690, https://doi.org/10.1073/pnas.0908741107

Busetto, L., Ranghetti, L., 2020. prismaread: A tool for facilitating access and analysis of prisma l1/l2 hyperspectral imagery. URL https://lbusett.github.io/prismaread/.

Cernicharo, J., Verger, A., & Camacho, F. (2013). Empirical and Physical Estimation of Canopy Water Content from CHRIS/PROBA Data. *Remote Sensing*, *5*, 5265–5284. https://doi.org/10.3390/rs5105265

D03 - State-of-the-art review report on
the EO analysis method/s and
algorithm/s

Champagne, C., Staenz, K., Beannari, A., Mcnairn, H. & Deguise, J. (2003). Validation of a hyperspectral curve-fitting model for the estimation of plant water content of agricultural canopies. Remote Sensing of Environment, 87, 148–160.

Cheng, Y., Zarco-Tejada, P., Riano, D., Rueda, C. &Ustin, S. (2006). Estimating vegetation water content with hyperspectral data for different canopy scenarios: Relationships between AVIRIS and MODIS indexes. Remote Sensing of Environment, 115, 354–366.

Clevers, J. G. P. W., Kooistra, L., & Schaepman, M. E. (2008). Using spectral information from the NIR water absorption features for the retrieval of canopy water content. *International Journal of Applied Earth Observation and Geoinformation*, *10*, 388–397. https://doi.org/10.1016/j.jag.2008.03.003

Clevers, J. G. P. W., Kooistra, L., & Schaepman, M. E. (2010). Estimating canopy water content using hyperspectral remote sensing data. *International Journal of Applied Earth Observation and Geoinformation*, *12*, 119–125. https://doi.org/10.1016/j.jag.2010.01.007

Dobrowski, S., Pushnik, J., Zarco-Tejada., P. & Ustin, S. (2005). Simple reflectance indices track heat and water stress-induced changes in steady-state chlorophyll fluorescence at the canopy scale. Remote Sensing of Environment, 97, 40–414.

Elsherbiny, O., Fan, Y., Zhou, L., & Qiu, Z. (2021). Fusion of Feature Selection Methods and Regression Algorithms for Predicting the Canopy Water Content of Rice Based on Hyperspectral Data. *Agriculture*, *11*, 51. https://doi.org/10.3390/agriculture11010051

Fong AY, Wachman E. (2008). Hyperspectral imaging for the life sciences. *Biophotonics Int.*,15:38.

Gerhards, M., Rock, G., Schlerf, M., & Udelhoven, T. (2016). Water stress detection in potato plants using leaf temperature, emissivity, and reflectance. *International Journal of Applied Earth Observation and Geoinformation*, *53*, 27–39. https://doi.org/10.1016/j.jag.2016.08.004

Green, R., Conel, J.& Roberts, D. (1993). Estimation of Aerosol Optical Depth and Additional Atmospheric Parameters for the Calculation of Apparent Reflectance from Radiance Measured by the Airborne Visible/Infrared Imaging Spectrometer. AVIRIS Proceedings October 25-29, 1993, JPL Publication, 93-26.

Guanter, L., Kaufmann, H., Segl, K., Foerster, S., Rogass, C., Chabrillat, S., Kuester, T., Hollstein, A., Rossner, G., Chlebek, C., Straif, C., Fischer, S., Schrader, S., Storch, T., Heiden, U., Mueller, A., Bachmann, M., Mühle, H., Müller, R., et al. (2015). The EnMAP Spaceborne Imaging Spectroscopy Mission for Earth Observation. *Remote Sensing*, *7*, 8830–8857. https://doi.org/10.3390/rs70708830

Hewison, T.J., 2001. Airborne measurements of forest and agricultural land surface emissivity at millimeter wavelengths. IEEE Trans. Geosci. Remote Sens. 39, 393–400.

Kato., A, et al. (2021), Assessing the inter-annual variability of vegetation phenological events observed from satellite vegetation index time series in dryland sites, Ecological Indicators, 130, 108042

Kersting K, Xu Z, Wahabzada M, Bauckhage C, Thurau C, Roemer C, et al. (2012). Pre-symptomatic prediction of plant drought stress using dirichlet-aggregation regression on hyperspectral images. AAAI. https://www.aaai.org/ocs/index.php/AAAI/AAAI12/paper/ view/4932.

Li, H., Yang, W., Lei, J., She, J., & Zhou, X. (2021). Estimation of leaf water content from hyperspectral data of different plant species by using three new spectral absorption indices. *PLOS ONE*, *16*, e0249351. https://doi.org/10.1371/journal.pone.0249351

D03 - State-of-the-art review report on
the EO analysis method/s and
algorithm/s

Loizzo, R., Daraio, M., Guarini, R., Longo, F., Lorusso, R., Dini, L., Lopinto, E., 2019. Prisma mission status and perspective, pp. 4503–4506.

Lowe, A., Harrison, N., & French, A. P. (2017). Hyperspectral image analysis techniques for the detection and classification of the early onset of plant disease and stress. *Plant Methods*, *13*, Article 1. https://doi.org/10.1186/s13007-017-0233-z

Lu, B., Dao, P., Liu, J., He, Y., & Shang, J. (2020). Recent Advances of Hyperspectral Imaging Technology and Applications in Agriculture. *Remote Sensing*, *12*, 2659. https://doi.org/10.3390/rs12162659

Masiello, G., Serio, C., Venafra, S., DeFeis, I., & Borbas, E. E. (2014). Diurnal variation in Sahara desert sand emissivity during the dry season from IASI observations. Journal of Geophysical Research: Atmospheres, 119, 1626–1638. https://doi.org/10.1002/jgrd.50863

Meerdink, S., Roberts, D., Hulley, G., Gader, P., Pisek, J., Adamson, K., King, J., Hook, S. J., 2019. Plant species' spectral emissivity and temperature using the hyperspectral thermal emission spectrometer (HyTES) sensor. Remote Sens. Environ. 224, 421–435.

Meerdink, S.K., Roberts, D.A., King, J.Y., Roth, K.L., Dennison, P.E., Amaral, C.H., Hook, S.J., 2016. Linking seasonal foliar traits to VSWIR-TIR spectroscopy across California ecosystems. Remote Sens. Environ. 186, 322–338.

Moshou D, Pantazi X-E, Kateris D, Gravalos I. (2014). Water stress detection based on optical multisensor fusion with a least squares support vector machine classifier. Biosyst Eng. 117:15–22.

Neinavaz, E., Darvishzadeh, R., Skidmore, A.K., Abdullah, H., 2019. Integration of landsat-8 thermal and visible-short wave infrared data for improving prediction accuracy of forest leaf area index. Remote Sensing 11, 390.

Neinavaz, E., Schlerf, M., Darvishzadeh, R., Gerhards, M., and Skidmore, A. K. (2021), Thermal infrared remote sensing of vegetation: Current status and perspectives, International Journal of Applied Earth Observation and Geoinformation, 102, 102415.

Peñuelas, J., Filella, I., Biel, C., Serrano, L., & Savé, R. (1993). The reflectance at the 950–970 nm region as an indicator of plant water status. *International Journal of Remote Sensing*, *14*, 1887–1905. https://doi.org/10.1080/01431169308954010

Pu, R., Ge, S., Kelly, M. & Gong, P. (2003). Spectral absorption features as indicators of water status in coast live oak (Quercus agrifolia) leaves. International Journal of Remote Sensing, 24(9), 1799–1810.

Rast, M., & Painter, T. H. (2019). Earth Observation Imaging Spectroscopy for Terrestrial Systems: An Overview of Its History, Techniques, and Applications of Its Missions. *Surveys in Geophysics*, *40*, 303–331. https://doi.org/10.1007/s10712-019-09517-z

Ribeiro da Luz, B., Crowley, J.K., 2010. Identification of plant species by using high spatial and spectral resolution thermal infrared (8.0–13.5 µm) imagery. Remote Sens. Environ. 114, 404–413.

Römer C, Wahabzada M, Ballvora A, Rossini M, Panigada C, Behmann J, et al. (2012). Early drought stress detection in cereals: simplex volume maximization for hyperspectral image analysis. Funct Plant Biol. 39:878–90.

D03 - State-of-the-art review report on
the EO analysis method/s and
algorithm/s

Running, S.W., Gower, S. (1991). Forest-BGC, a general model of forest ecosystem processes for regional applications. Ii. Dynamic carbon allocation and nitrogen budgets. Tree Physiol., 9, 147–160.

Segl, K., Kaufmann, H., H. Bach, Wagner, A., Hill, J., Heim, B., Oppermann, K., Heldens, W., Stein, E., Müller, A., van der Linden, S., Leitão, P. J., Rabe, A., & Hostert, P. (n.d.). Hyperspectral Algorithms.

Sims, D.& Gamon, J. (2003). Estimation of vegetation water content and photosynthetic tissue area from spectral reflectance: a comparison of indices based on liquid water and chlorophyll absorption features. Remote Sensing of Environment, 84, 526–537.

Sonnenschein, R., Jarmer, T., Vohland, M. & Werner, W. (2005). Spectral determination of plant water content of wheat canopies. Proceedings of 4th EARSeL Workshop on Imaging Spectroscopy,Warsaw.

Tagliabue, G., Boschetti, M., Bramati, G., Candiani, G., Colombo, R., Nutini, F., Pompilio, L., Rivera-Caicedo, J. P., Rossi, M., Rossini, M., Verrelst, J., & Panigada, C. (2022). Hybrid retrieval of crop traits from multi-temporal PRISMA hyperspectral imagery. *ISPRS Journal of Photogrammetry and Remote Sensing*, *187*, 362–377. https://doi.org/10.1016/j.isprsjprs.2022.03.014

Thurau C, Kersting K, Bauckhage C. (2010): Yes we can: simplex volume maximization for descriptive web-scale matrix factorization. In: Proceedings of 19th ACM international conference *on* information *and* knowledge management. New York, NY: ACM; p. 1785–8. http://doi.acm.org/10.1145/1871437.1871729.

Trombetti, M., Riano, D., Rubio, M., Cheng, Y.& Ustin, S. (2008). Multi-temporal vegetation canopy water content retrieval and interpretation using artificial neural networks for the continental USA. Remote Sensing of Environment, 112, 203–215.

Ullah, S., Groen, T.A., Schlerf, M., Skidmore, A.K., Nieuwenhuis, W., Vaiphasa, C., 2012. Using a genetic algorithm as an optimal band selector in the mid and thermal infrared (2.5–14 μm) to discriminate vegetation species. Sensors 12, 8755–8769.

Verhoef, W., Bach, H. (2007): Coupled soil-leaf-canopy and atmosphere radiative transfer modeling to simulate hyperspectral multi-angular surface reflectance and TOA radiance data; Remote Sensing of Environment, 109 (2007) 166–182

Verhoef, W., Bach, H. (2012): Simulation of Sentinel-3 images by four stream surface atmosphere radiative transfer modeling in the optical and thermal domains. In: Remote sensing of environment, 120 (2012) pp. 197-207.

Verrelst, J., Rivera-Caicedo, J. P., Reyes-Muñoz, P., Morata, M., Amin, E., Tagliabue, G., Panigada, C., Hank, T., & Berger, K. (2021). Mapping landscape canopy nitrogen content from space using PRISMA data. *ISPRS Journal of Photogrammetry and Remote Sensing*, *178*, 382–395. https://doi.org/10.1016/j.isprsjprs.2021.06.017

Vohland, M. (2008). Using imaging and non-imaging spectroradiometer data for the remote detection of vegetation water content. *Journal of Applied Remote Sensing*, *2*, 23520. https://doi.org/10.1117/1.2937937

Wocher, M., Berger, K., Danner, M., Mauser, W., & Hank, T. (2018). Physically-Based Retrieval of Canopy Equivalent Water Thickness Using Hyperspectral Data. *Remote Sensing*, *10*, 1924. https://doi.org/10.3390/rs10121924

Wutzler, T., Migliavacca, M., Julitta, T., 2016. FieldSpectroscopyCC: R package for Characterization and Calibration of spectrometers. R package version (5), 227.

D03 - State-of-the-art review report on
the EO analysis method/s and
algorithm/s

Yu F H Xu T Y, D. W. (2017). Radiative transfer models (RTMs) for field phenotypinginversion of rice based on UAV hyperspectral remote sensing. *Int J Agric & Biol Eng*, *10*, 150–157.

Yu, Y., et al., (2021), Interannual Spatiotemporal Variations of Land Surface Temperature in China From 2003 to 2018, IEEE Journal of Selected Topics in Applied Earth Observations and Remote Sensing, 14, 1783-1795, 2021, doi: 10.1109/JSTARS.2020.3048823.